Journal of Colloid and Interface Science 692 (2025) 137494

Contents lists available at ScienceDirect

Journal of Colloid And Interface Science

journal homepage: www.elsevier.com/locate/jcis

Cationic porphyrin-based covalent organic frameworks for enhanced phototherapy and targeted chemotherapy of bacterial infections

Jia-Jun Qian [a,b,c,1], Jing-Xuan Guo [d,1], Meng-Chao Wang [a,b,c], Li-Jian Chen [a,b,c], Xu Zhao [a,b,c,*], Xiu-Ping Yan [a,b,c]

[a] State Key Laboratory of Food Science and Resources, Jiangnan University, Wuxi 214122, China
[b] International Joint Laboratory on Food Safety, Jiangnan University, Wuxi 214122, China
[c] Institute of Analytical Food Safety, School of Food Science and Technology, Jiangnan University, Wuxi 214122, China
[d] Analysis and Testing Center, Jiangnan University, Wuxi 214122, China

HIGHLIGHTS

- A cationic COFs (TAPP-VIO) has been prepared as a non-antibiotic bactericide.
- TAPP-VIO features enhanced photo-therapy and targeted chemotherapy capabilities.
- TAPP-VIO produces 179 % more $^1O_2$ than nonionic porphyrin COF.
- TAPP-VIO induces an 85 % temperature rise compared to nonionic porphyrin COF.
- TAPP-VIO significantly promotes the healing of infected wounds.

GRAPHICAL ABSTRACT

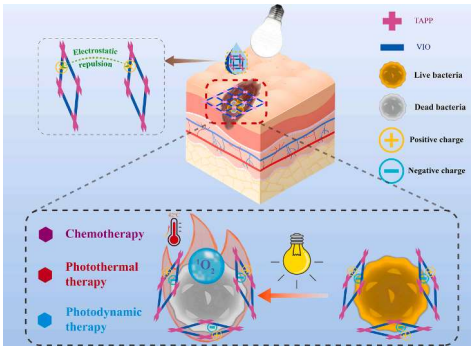

ARTICLE INFO

Keywords:
Cationic covalent organic frameworks
Bacterial targeting
Phototherapy
Bacterial infection

ABSTRACT

Bacterial infections significantly impede wound healing and threaten global public health. Porphyrin covalent organic frameworks (COFs) have shown promise as phototherapy antibacterial materials. However, the inherent π–π stacking interactions between the monomers also lead to aggregation and quenching of photosensitizers, thereby reducing the production of singlet oxygen ($^1O_2$) and compromising their antibacterial efficacy. Herein, we designed and prepared a novel cationic porphyrin-based COFs nanoplatform (TAPP-VIO), utilizing photo-sensitive TAPP and cationic VIO as structural units. This multifunctional nanoplatform is specifically tailored for targeted phototherapy and chemotherapy against bacterial infections. Upon irradiation, TAPP unit in TAPP-VIO generates heat and $^1O_2$, which effectively disrupt bacterial structure and cause cell death. The incorporation of VIO unit introduces electrostatic repulsion between layers, mitigating π-π stacking effects and enhancing $^1O_2$ production. Additionally, the positive charge imparted by the VIO unit enables TAPP-VIO to bind efficiently to negatively charged bacterial surfaces, immobilizing the bacteria and reducing their motility, thereby improving the overall efficacy of phototherapy. Under identical experimental conditions and concentrations, TAPP-VIO exhibits a $^1O_2$ generation capacity that is 179 % higher than that of nonionic porphyrin COF. Moreover, the

* Corresponding author at: State Key Laboratory of Food Science and Resources, Jiangnan University, Wuxi 214122, China.
E-mail address: zhaoxu2017@jiangnan.edu.cn (X. Zhao).
[1] These authors contributed equally to this work.

https://doi.org/10.1016/j.jcis.2025.137494
Received 27 January 2025; Received in revised form 28 March 2025; Accepted 31 March 2025
Available online 31 March 2025

temperature increase induced by TAPP-VIO is 85 % of that observed with nonionic porphyrin COF (TAPP-MMA-Da), which is conducive to enhancing the phototherapeutic effects while minimizing heat-induced damage to healthy tissues. In summary, our study presents a straightforward approach to developing non-antibiotic antibacterial nanoagents, and the as-prepared TAPP-VIO is a promising candidate drug suitable for clinical trials in the future.

1. Introduction

Skin, as a body primary tissue in contact with the external environment, plays a crucial role in maintaining internal stability and preventing the loss of water, electrolytes, and body fluids. Rapid wound healing is an important process for the repair of skin and other tissues [1]. However, bacteria in the environment can readily invade wounds during the healing process, potentially causing infections that slow down wound healing and may even lead to more serious tissue damage [2]. Antibiotics are currently the most widespread and effective treatment for bacterial diseases. However, since the late 20th century, overuse of antibiotics has led to the emergence of bacterial resistance, which is spreading at an alarming rate [3,4]. Chronic wound infections caused by drug-resistant bacteria have now become a serious threat to human health [5]. Therefore, the development of novel antibacterial drugs has become a research hotspot in the field of medicine [6–10].

Compared with typical antibiotic treatment, antibacterial technologies based on physical stimulation offer a more comprehensive and effective approach for combating both common and multidrug-resistant bacteria, potentially lowering the risk of bacterial resistance [11–13]. Among them, photodynamic therapy (PDT) has gained significant research interest due to its low toxicity, non-invasive, and negligible drug resistance. Upon laser irradiation, photosensitizers (PSs) can generate produce cytotoxic free radicals or singlet oxygen ($^1O_2$) to destroy essential components of bacteria, such as proteins, lipids, and nucleic acids, resulting in bacterial death, but its bactericidal effect often falls short of therapeutic expectations [14]. To enhance antibacterial efficacy, researchers are increasingly exploring synergistic antibacterial methods [15,16]. Hyperthermia generated by photothermal therapy (PTT) can weaken the cellular activity of bacteria, increasing their sensitivity to reactive oxygen species (ROS) and reducing the required ROS dosage for bacterial eradication [17]. Therefore, the combination of PDT and PTT is expected to improve antibacterial efficiency. Tetracyclic pyrrole compounds with synergistic PDT and PTT capabilities are regarded as one of the most promising PSs [18]. However, these traditional organic small molecule photosensitizers are often limited by the disadvantages of poor water solubility, self-quenching and low photostability. In this regard, it has become a research focus to find materials with good water solubility, strong dispersibility, and robust stability in vivo to enhance the clinical efficacy of PSs [19–22]. Furthermore, to further improve the bactericidal effect, the synthesis of bacteria-targeting antibacterial drugs without resistance has also become an urgent problem to be solved [23–25].

Covalent organic frameworks (COFs) are a new type of crystalline porous polymers with substantial application potential across various fields [26–28], owing to their simple design, well-defined structure, and tunable structural units that allow for functional diversity [29–33]. COFs have unique stability and excellent biocompatibility, and also show promising applications in the biomedical field [34–37]. In particular, the rigid and ordered structure of COFs offers an effective strategy for modulating the aggregation behavior PSs [38–40]. Additionally, relevant studies have demonstrated that the porous architecture of COFs also facilitates the generation and diffusion of $^1O_2$ [41–43]. In recent years, the application of COF structures in antibacterial phototherapy has garnered significant attention [44,45]. However, the inherent hydrophobicity and the regular layered stacking of COF lead to a certain degree of aggregation among monomers in the biological environment, which still restricts the production of ROS, thereby reducing the effectiveness of in vivo PDT [44,46,47]. Besides, the layer by layer stacking effect of COF often results in surplus photothermal properties, which may cause thermal damage to adjacent tissues [48,49]. Therefore, developing a feasible strategy to synthesize COFs with enhanced photodynamic properties and moderate photothermal properties, further improving their therapeutic efficacy and minimizing potential side effects is of paramount importance. Cationic groups exhibit inherent bacteria-targeting and bactericidal properties [50,51], making them attractive candidates for enhancing the therapeutic performance of COFs. Specifically, the incorporation of cationic groups is anticipated to increase the electrostatic repulsion between the layers of COFs, thereby optimizing their phototherapy efficacy. However, the construction of cationic COFs that can achieve the ideal phototherapy efficacy remains a significant challenge.

Herein, we report a cationic COF (TAPP-VIO) multifunctional nanoplatform for bacteria-targeted and efficient chemotherapy/phototherapy sterilization and wound healing. The nanoplatform was synthesized via a Schiff base condensation reaction using photosensitizer 5,10,15,20-tetra (4-aminophenyl) porphyrin (TAPP) and cationic compound 1,1′- benzaldehyde 4,4′-bipyridinium (VIO) as structural units. TAPP unit provides excellent $^1O_2$ generation ability and moderate photothermal conversion under white light irradiation. VIO unit introduces certain electrostatic repulsion between the layers, which reduces the π-π stacking effect and thereby enhances the phototherapy performance of the COF. In addition, the positive charge of VIO allows it to interact with the negatively charged membrane surface of bacteria, thereby immobilizing the bacteria, limiting their mobility, and enhancing the effective contact between TAPP-VIO and bacteria. The strong binding also mitigates, to some extent, the insufficient phototherapeutic efficiency caused by the short half-life of $^1O_2$ [52], which is beneficial to the improvement of the therapeutic efficiency of TAPP-VIO. Compared with the reported porphyrin COF (at the same concentration and conditions), cationic TAPP-VIO exhibits a higher $^1O_2$ generation capacity and relatively mild photothermal effect (the $^1O_2$ generation capacity is 179 % of the porphyrin COF, while the temperature rise is 85 % of porphyrin COF). In the plate experiment, TAPP-VIO (5.00×10^{-4} g mL^{-1}) combined with irradiation (100 mW cm^{-2}) reduced the number of Staphylococcus aureus (*S. aureus*) colonies to 0.81 % and Escherichia coli (*E. coli*) colonies to 1.16 % of the control group. In addition, TAPP-VIO also has a good ability to promote wound healing without significant side-effects in bacteria-infected mouse model. The as-prepared TAPP-VIO exhibits better bactericidal properties and broader application prospects. The proposed preparation strategy of multifunctional antibacterial platform provides a new pathway for the development of high-performance antibacterial agents.

2. Materials and methods

2.1. Materials

All chemicals and reagents are analytical grade or above. Tetrahydrofuran (THF), acetic acid, *N,N*-dimethylformamide (DMF), ethanol (EtOH), mesitylene and acetonitrile (ACN) were purchased from China National Pharmaceutical Group Chemical Reagent Co., Ltd. (Shanghai, China). 2,5-Di-(2-methyl methacrylate) *p*-benzaldehyde (MMA-Da), VIO and TAPP were provided by Jilin Chinese Academy of Sciences-Yanshen Technology Co., Ltd. (Jilin, China). 9,10-Anthracenediyl-bis(methylene) dimalonic acid (ABDA) and o-dichlorobenzene (o-DCB) were purchased

from Macklin Biochemical Co., Ltd. (Shanghai, China). Ultrapure water was provided by Wahaha Group Co., Ltd. (Hangzhou, China). The premixed powder of phosphate buffer saline (PBS) solution, LB Agar powder (FMB Grade), and Luria-Bertani (LB) meat soup powder (FMB grade) were provided by Shanghai Sangon Biotech (Shanghai, China). 2′,7′-Dichlorodihydrofluorescein diacetate (DCFH-DA) was provided by Aladdin Biochemical Technology Co., Ltd. (Shanghai, China). Calcein acetoxymethyl ester (Calcein-AM)/propidium iodide (PI) double stain kit was purchased from Yeason Biotechnology Co. (Shanghai, China). *S. aureus*(ATCC 25923) and *E. coli* (ATCC 25922) were frozen bacteria in our laboratory.

2.2. Synthesis of TAPP-VIO

The preparation of TAPP-VIO is briefly described below. TAPP (16.8 mg, 0.025 mmol), VIO (21.9 mg, 0.050 mmol) and BuOH/Mesitylene solution (1/1, v/v, 2.00 mL) were first added to a Pyrex tube and sonicated for 5 min, then 0.20 mL of acetic acid was added and sonicated again for 5 min. The mixture in the tube was then degassed (three freeze–pump–thaw cycles) and sealed. The resulting mixture was then stirred at 120 °C for 6 days followed by centrifuged after cooled to room temperature. The targeted product (TAPP-VIO) was then obtained by washing five times with THF and drying under vacuum at 50 °C.

For comparison, a nonionic porphyrin COF (TAPP-MMA-Da) was synthesized according to our previous report [53].

2.3. Photodynamic and photothermal properties of TAPP-VIO

To evaluate the photodynamic performance of TAPP-VIO, ABDA was selected as the $^1O_2$ indicator. Firstly, 10.00 mL of mixed solutions of ABDA (5.00×10^{-5} mol L^{-1}) and TAPP-VIO with different concentrations (0.00, 1.25, 2.50, 5.00, and 7.50×10^{-4} g mL^{-1}, respectively) were configured in 50 mL centrifuge tubes. The solution was then exposured to a white LED lamp (50, 100, or 150 mW cm^{-2}) for different times (0, 2.5, 5, 7.5, 10, 12.5, 15, 17.5, and 20 min). After irradiation, 1.00 mL of solution was removed and centrifuged from each tube, and the then UV–Vis absorption spectrum of the resulting suspension was measured by UV–Vis–NIR spectrophotometer.

To investigate the photothermal properties of TAPP-VIO, different amounts of TAPP-VIO was dispersed in PBS to make the desired solution (1.25, 2.50, 5.00 and 7.50×10^{-4} g mL^{-1}, respectively). Then each solution (1.00 mL) was transferred to 48-well cell culture plate and irradiated with white LED lamp for 20 min. The same irradiation was performed with 1.00 mL of PBS as a control. The temperature change during irradiation was recorded by FLIR-50 thermal camera.

To clearly verify the effect of cationization on photodynamic and photothermal properties, TAPP monomer (2.22×10^{-4} g mL^{-1}) and TAPP-MMA-DA (4.00×10^{-4} g mL^{-1}) were selected as controls to repeat the above experiments, where the amount of TAPP was the same as that of TAPP-VIO (5.00×10^{-4} g mL^{-1}).

2.4. Bacterial cultures and antibacterial experiment

The bactericidal performance of TAPP-VIO was evaluated using *E. coli* and *S. aureus* as model bacteria. Firstly, the frozen bacteria were resuscitated to prepare a PBS bacterial suspension (10^8 CFU mL^{-1}). The experiment was then conducted by the following groups (1) Experimental group: 100 μL of bacterial suspension was added to PBS containing TAPP-VIO (final concentration of TAPP-VIO was 5.00×10^{-4} g mL^{-1}). After 30-min shaking and incubating (200 RPM, 37 °C), the bacterial suspension was irradiated under a white LED light (100 mW cm^{-2}) for different times (0, 10 and 20 min). (2) Control group: The bacterial suspension was incubated in PBS for 30 min, followed by exposure to 20-min irradiation (100 mW cm^{-2}). (3) Blank group: The same bacterial suspension was incubated in PBS without any treatment. At the end of the grouping, the bacterial suspension of each group was diluted 10^4 times in a stepwise manner, respectively. Then, 100 μL of the above diluted suspension was uniformly coated on the Luria-Bertani broth agar plates and incubated at 37 °C for 24 h. Finally, the number of colonies was counted and the bacterial survival rate was calculated.

Bacterial survival rate% = (number of colonies in experimental or control group/number of colonies in blank group) * 100.

2.5. Staining analysis and morphological observation

To further investigate the bactericidal effect of TAPP-VIO, staining analysis was carried out with Double Staining Kit (calcein acetoxymethyl ester/propidium iodide, Calcein-AM/PI). Briefly, the bacterial suspensions of each group were respectively stained with 100 μmol L^{-1} Calcein-AM and 4.50 μmol L^{-1} PI in the dark for 20 min, then centrifuged and resuspended with 20 μL PBS. 10 μL re-suspension was dropped into a slide coated with an anti-fluorescence quenching agent and fixed for 3–5 min before observation with confocal laser scanning microscope (CLSM).

The morphology of treated bacteria was further observed by scanning electron microscopy (SEM). For this purpose, 100 μL of bacterial suspension (10^8 CFU mL^{-1}) was mixed with 900 μL of PBS containing TAPP-VIO (final concentration was 5.00×10^{-4} g mL^{-1}) or not. The bacterial suspension was cultured for 30 min at 37 °C in the dark, and then irradiated with 100 mW cm^{-2} white LED light for different times (0, 10 and 20 min, respectively). The bacterial suspensions were the centrifuged (5000 rpm for 10 min) and immobilized. The suspensions were fixed with 2.5 % glutaraldehyde (20 h), washed twice with PBS, and then gradient dehydrated with 30 %, 50 %, 70 %, 80 %, 95 % and 100 % (v/v) EtOH solution for 10 min. Finally, the resulting bacteria were frozen for 12 h at −20 °C and −80 °C, and their morphology was observed by SEM after lyophilization.

2.6. Detection of intracellular $^1O_2$ in bacteria

DCFH-DA was selected as the intracellular $^1O_2$ detection probe to further verify the photodynamic bactericidal mechanism of TAPP-VIO. Specifically, 100 μL of bacterial suspension (*E. coli* and *S. aureus*: 10^8 CFU mL^{-1}) was treated as follows. (1) Experimental group: 100 μL bacterial suspension was mixed with TAPP-VIO and DCFH-DA solutions with final concentrations of 5.00×10^{-4} g mL^{-1} and 10 μmol L^{-1}, respectively, and the final volume was fixed to 10 mL. (2) Control group: bacterial suspension was incubated with DCFH-DA only, and other conditions were the same as in the experimental group. After 30-min incubation at 37 °C, the above bacterial suspension was irradiated with a white LED light (100 mW cm^{-2}) for different times (0, 10 and 20 min). After centrifugation (5000 rpm, 10 min), the bacterial suspension was resuspended in PBS (20 μL). Finally, 10 μL of the suspension was added dropwise to a glass slide and images were acquired using CLSM at 488 nm laser.

2.7. Murine infection model and antibacterial application

To investigate the synergistic bactericidal and wound-healing effects of TAPP-VIO via photothermal, photodynamic, and chemical mechanisms, a model of *S. aureus* infection was established in female BALB/c mice aged 5–6 weeks, followed by subsequent experiments. Initially, a circular skin wound (diameter ≈ 7 mm) was created on the back of each mouse, and 10.0 μL of *S. aureus* suspension was applied topically. One day post-infection, mice were randomly assigned to four groups (n = 5): (1) no treatment. (2) coating of TAPP-VIO (5.00×10^{-4} g mL^{-1}, 50.0 μL) on the wound. (3) irradiated with white LED light at 100 mW cm^{-2} for 20 min. (4) combination treatment with TAPP-VIO (5.00×10^{-4} g mL^{-1}, 50.0 μL) and 100 mW cm^{-2} of white LED light for 20 min. The wound-

healing promotion effect of TAPP-VIO was evaluated by monitoring the body weight, wound status and wound area of the mice on a daily basis until complete healing occurred in the treatment group. All animal experiments adhered strictly to protocols approved by the Institutional Animal Care and Use Committee of Jiangnan University (JN.No. No20220430b0180606[147]).

The biosafety and antibacterial effects of TAPP-VIO were further evaluated through masson and haematoxylin and eosin (H&E) staining and immunohistochemical analysis of major organs and wound tissues. Briefly, mice were sacrificed at the end of experiment. Major organs (lung, spleen kidney, liver and heart) and wound tissues were harvested and immobilized with 4 % paraformaldehyde. H&E staining and histochemical analysis (including interleukin-6 (IL-6) and tumor necrosis factor-α (TNF-α)) were then performed.

3. Results and discussion

3.1. Design, preparation and characterization of TAPP-VIO

The design and preparation of the cationic COF nanoplatform TAPP-VIO for targeted phototherapy and chemotherapy of bacterial infections are shown in Scheme 1. To achieve an ideal bacteria-targeted synergistic phototherapy with enhanced photodynamic properties and relatively mild photothermal effects, photosensitizer TAPP and cationic VIO are employed as structural units to construct the bacteria-targeted cationic COF (TAPP-VIO) nanoplatform through a Schiff base condensation reaction. Specifically, The TAPP unit in TAPP-VIO can generate heat and $^1O_2$ upon illumination, which can destroy the bacterial structure and lead to their death. Meanwhile, VIO serves a dual function unit: On the one hand, it introduces a certain electrostatic repulsion between layer and layer, reducing the π–π stacking effect and facilitating the generation of $^1O_2$. On the other hand, its positive charge enables interaction with the negatively charged bacterial membrane, immobilizing the bacteria and hindering their migration. Membrane potential balance of bacteria will be broken also, makes TAPP-VIO closer to the bacteria, thereby enhancing the ROS-mediated bacterial killing effect. Compared to previously reported porphyrin-based COF, the cationic COF is expected to minimize the π-π stacking effect between PSs, enabling more efficient transfer of light energy to $^1O_2$, while reducing the thermal effect and limiting thermal damage to normal tissues. We believe that the as-prepared TAPP-VIO platform can provide valuable insights for the design of nano bactericidal materials in the future.

The ordered crystal structure of TAPP-VIO is conducive to the dispersion of TAPP unit and prevents its self-aggregation-induced quenching. The uniform porosity also contributes to the generation of ROS and improving the efficiency of PDT. Therefore, the synthesis conditions of TAPP-VIO, including solvent, temperature and time were first optimized. The crystallinity of TAPP-VIO was assessed using powder X-ray diffraction pattern (PXRD). Among the optimized six solvent systems (Fig. S1 and Fig. S1), the PXRD spectrum of TAPP-VIO showed an obvious characteristic peak at 3.5° only in the mesitylene/*n*-butanol reaction system. And the intensity of the characteristic peak was greatly affected by the mesitylene to *n*-butanol ratio, reaction temperature and time. To verify whether the characteristic peak at 3.5° corresponds to TAPP-VIO with a regular crystal structure, the structure of the designed TAPP-VIO was simulated by software. The experimental PXRD pattern of TAPP-VIO matched the characteristic peak of AA stacking predicted by the software simulation (Fig. 1a), confirming that the synthesized TAPP-VIO possesses a well-defined crystal structure. Besides, transmission electron microscope (TEM) and high resolution transmission electron microscopy (HR-TEM) images further demonstrate that TAPP-VIO exhibits a lamellar structure with well-ordered crystalline characteristics (Fig. 1b).

The successful preparation of TAPP-VIO was further characterized by Fourier transform infrared (FT-IR) spectroscopy. The appearance of the characteristic peak of –C=N– at 1671 cm^{-1} in the FT-IR spectrum of TAPP-VIO, as well as the concomitant disappearance of the characteristic bands of $–NH_2$ and –CHO groups (at 3327, 3348 cm^{-1} and 1703 cm^{-1}) form the original building monomers TAPP and VIO respectively, revealed the successful synthesis of TAPP-VIO (Fig. 1c). Then, the

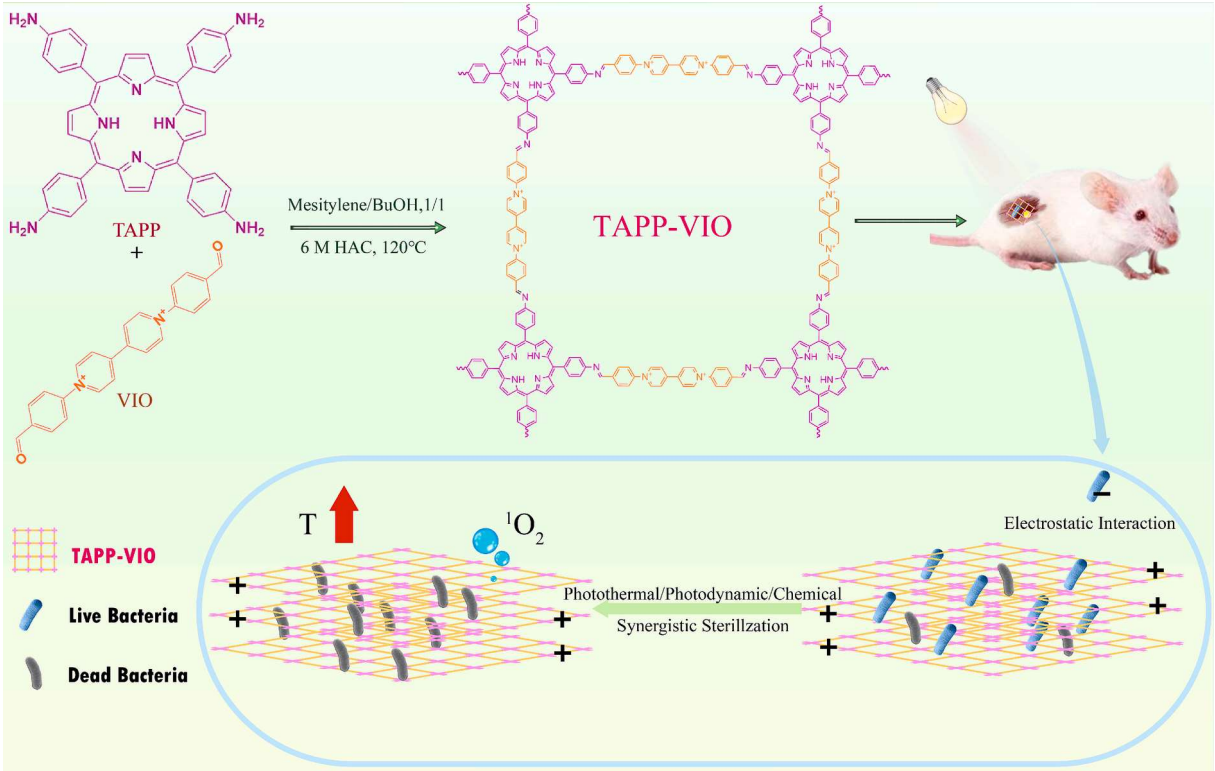

Scheme 1. The design strategy and schematic of TAPP-VIO for enhanced phototherapy and targeted chemotherapy of bacterial infections.

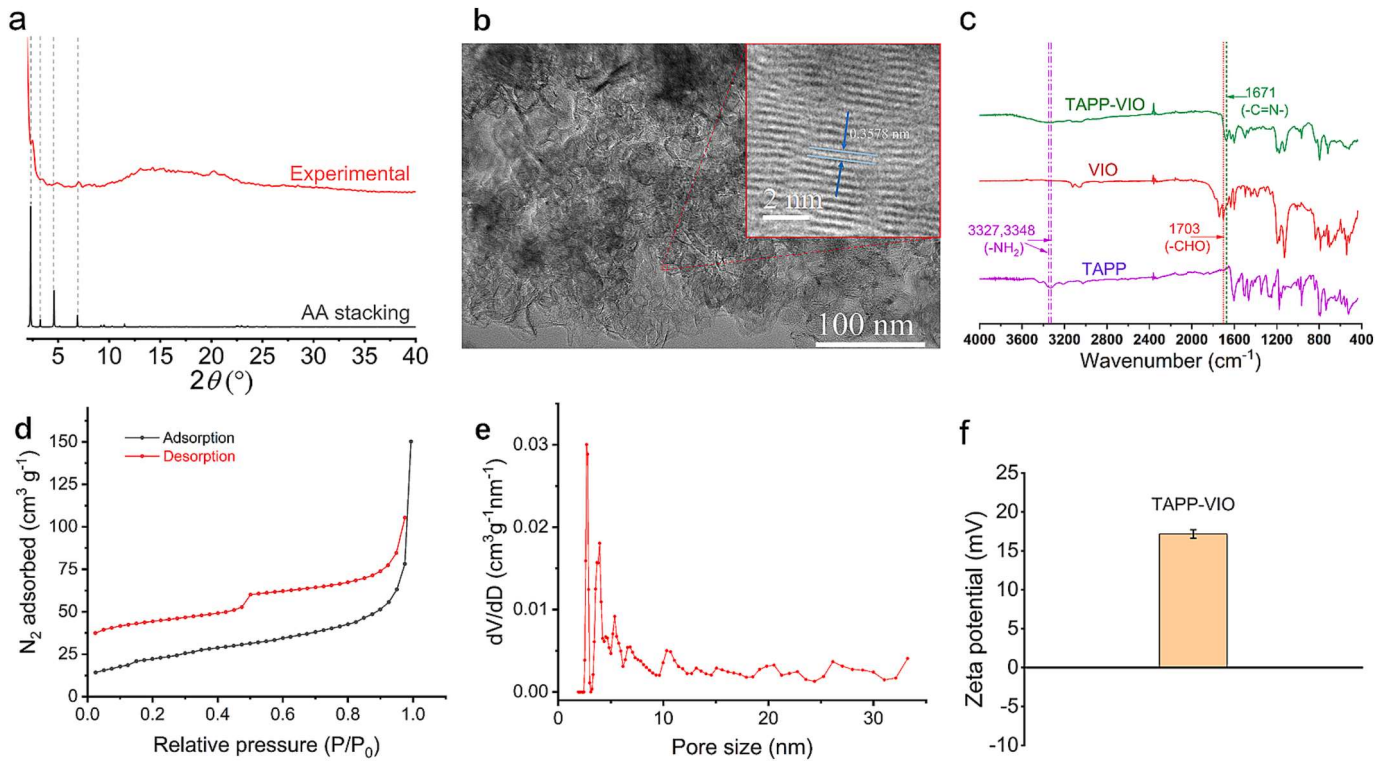

Fig. 1. (a)The simulated (AA stacking models) and experimental PXRD patterns of TAPP-VIO. (b) TEM and HR-TEM image of TAPP-VIO. (c) FT-IR spectra of TAPP-VIO, VIO and TAPP. (d) The N_2 adsorption–desorption isotherms of TAPP-VIO. (e) Pore size distribution of TAPP-VIO. (f) Zeta potential of TAPP-VIO in aqueous solution.

porosity of TAPP-VIO were characterized by N_2 adsorption isotherm. The prepared TAPP-VIO has a mesoporous structure with a Brunauer Emmett Teller (BET) surface areas of 78 $m^2\ g^{-1}$ (Fig. 1d) and an average pore size of 2.7 nm structure (Fig. 1e). Meanwhile, solid-state UV–Vis–NIR absorption spectroscopy showed a broad absorption band across the visible light region (Fig. S3), indicating the formation of a new conjugated system, which further confirms the successful synthesis of the TAPP-VIO. In addition, the zeta potential of TAPP-VIO aqueous solution was measured to be 17.2 ± 0.5 mV, indicating its positive charge. (Fig. 1f). This positive charge endows TAPP-VIO with superior dispersibility in water (Fig. S4), outperforming non-ionic COFs (TAPP-MMA-Da, prepared with slight modifications according to our previous report [53]). Furthermore, TAPP-VIO demonstrates remarkable thermal stability (Fig. S5). The porous lamellar structure, large BET surface area, broad absorption peak within the visible light range, excellent water dispersibility, and notable thermal stability collectively demonstrate that TAPP-VIO holds significant potential for phototherapeutic antibacterial applications.

3.2. *Photodynamic and photothermal properties of TAPP-VIO*

To evaluate the phototherapy bactericidal performance of TAPP-VIO, the photodynamic property of TAPP-VIO in aqueous solution was first investigated via ABDA as $^1O_2$ indicator. When only ABDA was present in the solution, the absorbance of ABDA at 377 nm did not decrease significantly even under 20 min of white light irradiation, indicating that ABDA itself was stable under this experimental condition (Fig. 2a and Fig. S6). While the absorbance of ABDA solution containing TAPP-VIO decreased significantly upon irradiation, confirming the generation of $^1O_2$. Meanwhile, the rate of decrease in ABDA absorbance was positively correlated with the concentration of TAPP-VIO ((Fig. 2a and Fig. S6), power density of irradiation (Fig. 2b and Fig. S7) and the exposure time (Fig. 2a, b and Fig. S7). After treatment with different concentrations of TAPP-VIO (1.25×10^{-4}, 2.50×10^{-4}, 5.00×10^{-4} and 7.50×10^{-4} g mL^{-1}) followed by 20-min white LED irradiation, the absorbance of ABDA decreased to 69 %、42 %、20 % and 7 % of the initial value, respectively (Fig. 2a and Fig.S6). However, no significant change in the absorbance of TAPP solution (2.22×10^{-4} g mL^{-1}, equivalent to 5.00×10^{-4} g mL^{-1} of TAPP-VIO) was observed under the same exposure (Fig. 2c and Fig. S7). The above results clearly imply that the ordered structure of TAPP-VIO effectively avoids the self-quenching of TAPP in aqueous solutions, thereby ensuring its $^1O_2$ generation capacity.

To further verify whether the introduction of the cationic monomer VIO enhances the photodynamic performance, the $^1O_2$ generation ability of non-ionic COF TAPP-MMA-Da was determined under the same irradiation and at the same molar concentration of TAPP (TAPP-MMA-Da, 4.00×10^{-4} g mL^{-1}, equivalent to TAPP-VIO 5.00×10^{-4} g mL^{-1}). The results showed that the rate of decrease in ABDA absorbance in the TAPP-VIO treatment group was significantly faster than that in the TAPP-MMA-Da treatment group (Fig. 2c and Fig. S8). After 20 min of irradiation, the absorbance in the TAPP-MMA-Da group decreased by only 56 % of that in the TAPP-VIO group (to 55 % and 20 % of the initial absorbance, respectively). These results indicate that TTAP-VIO does have better $^1O_2$ generation capacity than TAPP-MMA-Da. This enhanced performance can be attributed to the positive charge carried by TAPP-VIO, which reduces the π-π stacking effect in its COF structure, allowing more efficient transmission of light energy to O_2, and thus improving its photodynamic performance.

The photothermal effect of TAPP-VIO in PBS under white LED irradiation was then investigated. TAPP-VIO solution exhibited a temperature increase in relation to irradiation time, power density and concentration (Fig. 2d, e and Figs. S9–S10). After treatment with different concentrations of TAPP-VIO (1.25×10^{-4}, 2.50×10^{-4}, 5.00×10^{-4} and 7.50×10^{-4} g mL^{-1}) followed by 20-min white LED irradiation, the solution temperature increased to 35 °C, 37 °C, 42 °C, and 44 °C, respectively (Fig. 2d and Fig. S9). As documented in the literature [54,55], an optimal temperature of 42 °C is deemed suitable for mild

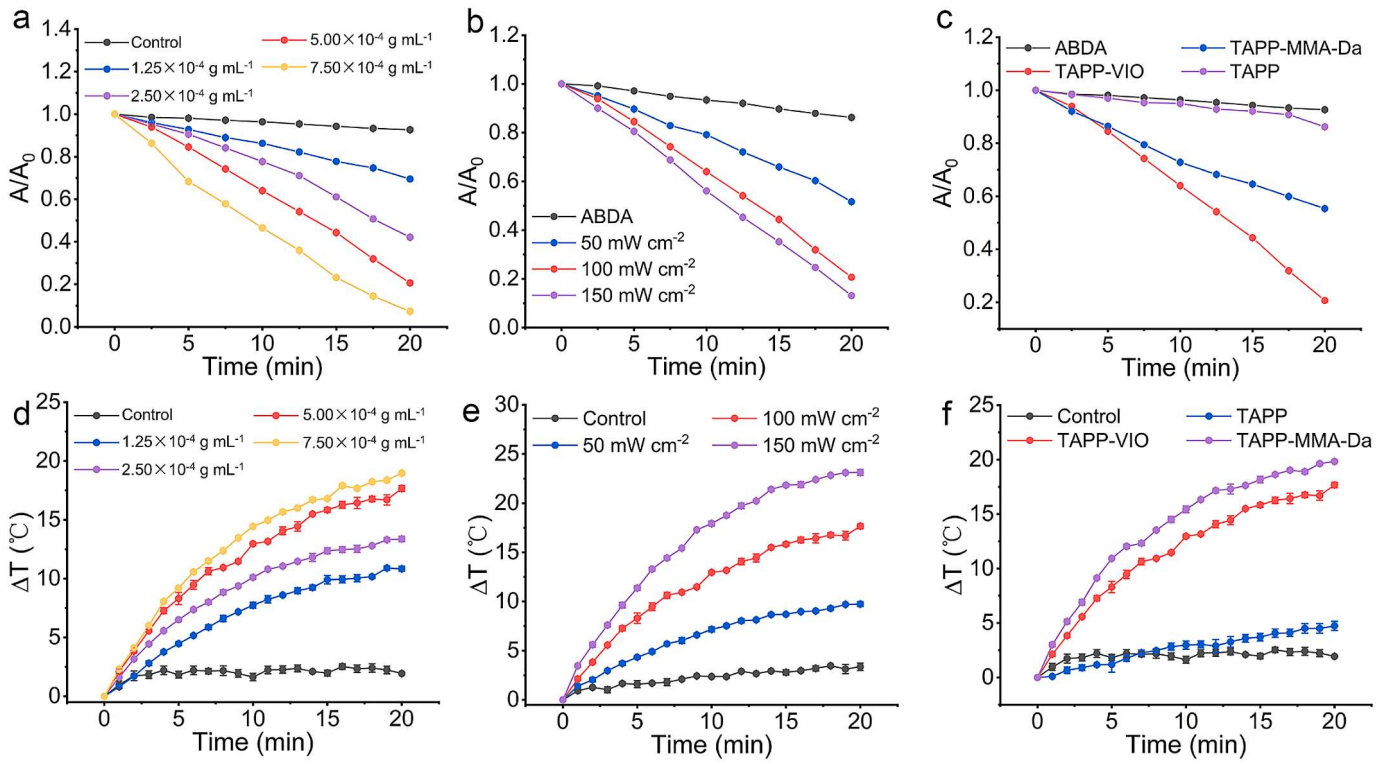

Fig. 2. (a) Time-dependent absorbance of ABDA (A/A_0) at maximum wavelength (377 nm) with different concentrations of TAPP-VIO or not under irradiation (100 mW cm^{-2}). (b) Relative change of absorbance (A/A_0) of ABDA at 377 nm with TAPP-VIO (500 μg mL^{-1}) under different powers of irradiation. (c)Time-dependent absorbance of ABDA (A/A_0) at 377 nm with different solutions (2.22×10^{-4} g mL^{-1} TAPP, 5.00×10^{-4} g mL^{-1} TAPP-VIO and 4.00×10^{-4} g mL^{-1} TAPP-MMA-Da, as equivalent TAPP) under irradiation (100 mW cm^{-2}). A_0 and A are the absorbance of ABDA before treatment for a certain time, respectively. (d) Time-dependent temperature changes of TAPP-VIO with different concentrations when irradiated by White LED (100 mW cm^{-2}). (e) Effect of irradiation power on the temperature of TAPP-VIO (5.00×10^{-4} g mL^{-1}). (f)Time-dependent temperature changes of different solutions (2.22×10^{-4} g mL^{-1} TAPP, 5.00×10^{-4} g mL^{-1} TAPP-VIO and 4.00×10^{-4} g mL^{-1} TAPP-MMA-Da) under the same powers of irradiation.

photothermal therapy. To balance the therapeutic efficacy of phototherapy with the minimization of thermal damage to normal tissues due to hyperthermia, while also considering potential toxicity, side effects, and cost in practical applications, TAPP-VIO concentration of 5.00×10^{-4} g mL^{-1} was ultimately selected for further investigation. Importantly, TAPP-VIO exhibited a milder photothermal effect ($\Delta T = 17$ °C) compared to TAPP-MMA-DA ($\Delta T = 20$ °C) with equivalent concentrations (molar concentration of TAPP) (Fig. 2F and Fig. S11). Moreover, the photothermal conversion efficiency of TAPP-VIO (19.93 %) was lower than that of other porphyrin-based COFs (Supplementary Data Table 1) [56,57]. These imply that the cationic framework structure of TAPP-VIO contributes to reducing thermal damage to adjacent normal tissues. In contrast, TAPP (2.22×10^{-4} g mL^{-1}, equivalent to 5.00×10^{-4} g mL^{-1} of TAPP-VIO) and PBS did not show a significant temperature increase even after 20-min irradiation at the same power density ($\Delta T = 5$ °C for TAPP and 2 °C for PBS) (Fig. 2F and Fig. S11). The above results confirm that the cationic framework structure of TAPP-VIO effectively reduces the strong π-π stacking effect between the COF layers, leading to enhanced photodynamic performance while minimizing excessive heat generation, which is more conducive to antibacterial applications.

3.3. *In vitro phototherapy/chemotherapy bactericidal effect of TAPP-VIO*

To evaluate the phototherapeutic antibacterial potential of TAPP-VIO, typical Gram-negative *E. coli* and Gram-positive *S. aureus* were selected as model pathogens for antibacterial experiments. The synergetic bactericidal effect of TAPP-VIO was firstly evaluated through the plate method with bacterial solutions (1×10^8 CFU mL^{-1}) of *S. aureus* and *E. coli*. The survival rate of both *S. aureus* and *E. coli* upon white LED irradiation (100 mW cm^{-2}) did not differ from that of the control group without any treatment (Fig. 3a, b and Fig. S12), indicating that the selected power density and exposure time did not cause irreparable damage to the bacteria. While the survival rate of above two typical pathogens was slightly reduced when treated with TAPP-VIO alone. This can be attributed to the ionic nature of TAPP-VIO, which carries a significant positive charge, allowing it to fix on the bacterial surfaces and break the balance of the bacterial membrane potential. Markedly, the bacterial survival rate in TTAP-VIO combined with irradiation treatment group was significantly reduced in a time-dependent manner. When the irradiation time was up to 20 min, nearly all of the *S. aureus* and *E. coli* were killed (Fig. 3a, b and Fig. S12). To sum up, TAPP-VIO not only has a certain bactericidal effect by itself, but its phototherapy bactericidal performance can also be activated by laser irradiation, showing excellent photothermal/photodynamic/chemical synergistic antibacterial performance. In summary, compared with non-ionic porphyrin COFs [53,58], TAPP-VIO exhibits superior antibacterial performance and lower photothermal temperatures under milder irradiation conditions, showing excellent potential for antibacterial applications.

To further investigate the synergetic bactericidal effect of TAPP-VIO, Calcein-AM/PI were subsequently chosen as probes to respectively label live (green fluorescence) and dead bacteria (red fluorescence) after different treatment. Confocal images of bacterial suspensions subjected to various treatments were consistent with the results of the plate experiment above (Fig. 3c). Notably, the uniformly dispersed fluorescence of *S. aureus* suspension, whether exposed to white LED or not, changed to an aggregated state as long as it was treated with TAPP-VIO (Fig. 3c). This aggregation likely results from the positively charged TAPP-VIO attracts and binds to the negatively charged *S. aureus*, thereby causing uniformly dispersed *S. aureus* to cluster around TAPP-VIO.

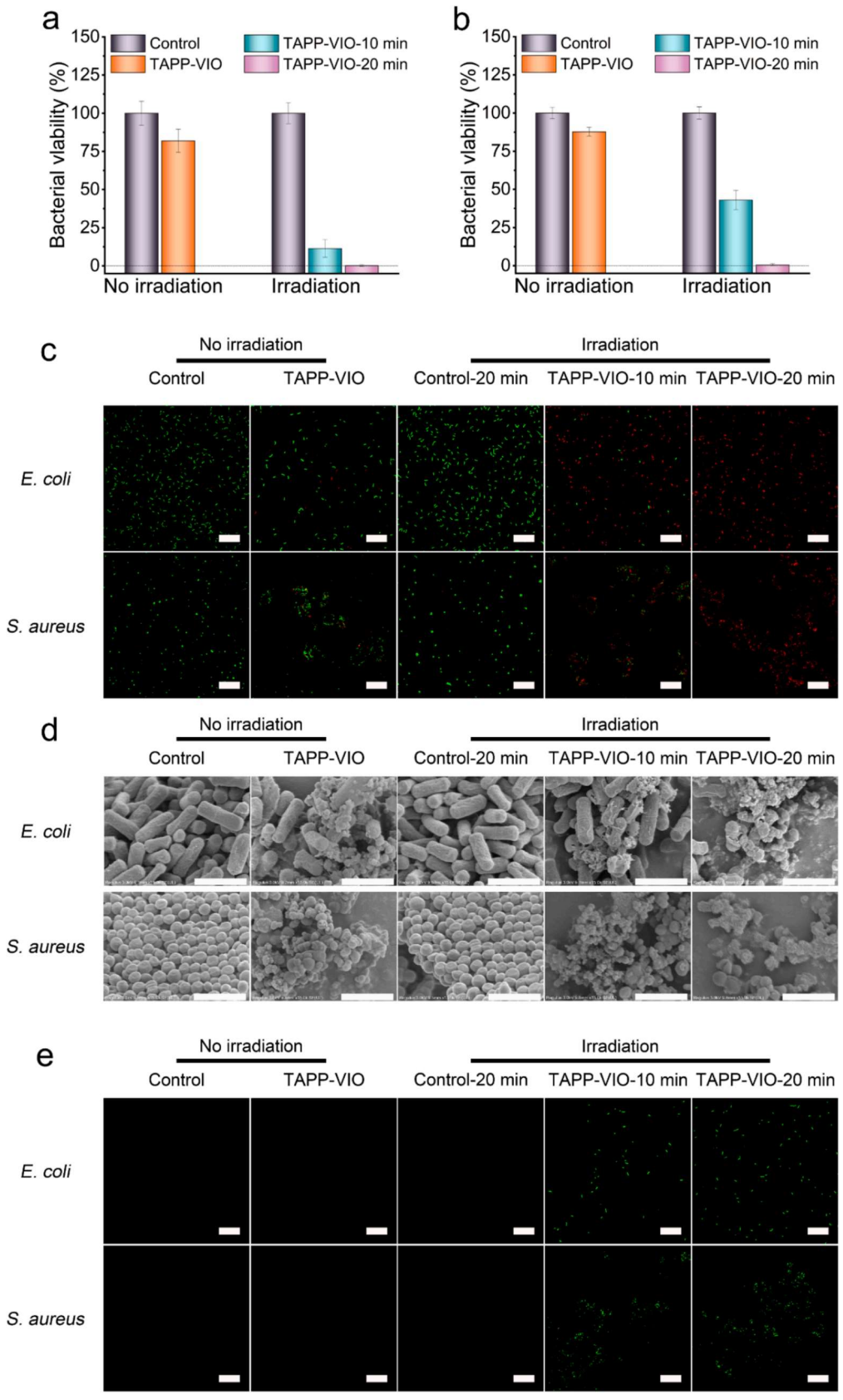

Fig. 3. The bactericidal effect of TAPP-VIO (5.00×10^{-4} g mL^{-1}) toward (a) *E. coli* and (b) *S. aureus* (statistical significance: * $P < 0.05$ and ** $P < 0.01$). (c) Confocal laser scanning microscopy (CLSM) imaging of *E. coli* and *S. aureus* after different treatments. Live and dead bacteria were stained in green and red by Calcein-AM and PI, respectively (scale bar, 30 μm). (d) The SEM images of bacteria after different treatments (scale bar, 3 μm). (e) The CLSM images of bacteria after different treatments for the detection of $^1O_2$ (scale bar, 30 μm).

Furthermore, this finding also confirms the bacteria-targeting of TAPP-VIO.

Scanning electron microscopy (SEM) was further employed to investigate the morphological changes of bacterial cells after different treatments. In both control group without any treatment and the irradiation-only group, the bacterial cells appeared full, smooth, and free from visible wrinkles (Fig. 3d). After TAPP-VIO treatment, however, TAPP-VIO adhered to the surface of the bacterial bodies, causing rupture. Moreover, TAPP-VIO combined with irradiation resulted in significant content leakage and morphological changes in the bacterial cells. These results indicate that TAPP-VIO adheres to the surface of bacteria and exerts a good bactericidal effect in situ upon light exposure.

To further verify the synergistic bactericidal mechanism, DCFH-DA was used as a $^1O_2$ indicator to verify the production of $^1O_2$ in the bacteria. DCFH-DA itself is non-fluorescent, but can be hydrolyzed by intracellular esterases and subsequently oxidized by $^1O_2$ to form green fluorescent product. In all of the above treatment groups, green fluorescence appeared only in the experimental group of bacteria treated with both TAPP-VIO and laser irradiation, and the fluorescence intensity increased with irradiation time (Fig. 3e). This indicates that only laser irradiation or TAPP-VIO treatment does not produce $^1O_2$, while $^1O_2$, can be produced if and only when both TAPP-VIO and laser illumination are applied.

3.4. *In vivo antibacterial effects of TAPP-VIO*

Inspired by the above in vitro excellent bactericidal ability of TAPP-VIO, in vivo phototherapy/chemical synergistic therapeutic performance of TAPP-VIO was explored using *S. aureus*-infected mouse model. The bio-compatibility of TAPP-VIO was firstly investigated through hemolytic assays. As shown in Fig. S13, the hemolysis rate of red blood cells remained below 1 % even the concentration of TAPP-VIO reached 750 μg mL^{-1}, indicating that TAPP-VIO has excellent biocompatibility and can be used for the treatment of infected wounds. To verify the in vivo therapeutic effect, *S. aureus*-infected mice were randomly divided into four groups, and the changes in body weight, behavior and wound area of mice during treatment were recorded. TAPP-VIO was dropped into the wound and irradiated with white LED as the treatment experiment, while the control group was no treatment, laser irradiation or TAPP-VIO treatment only.

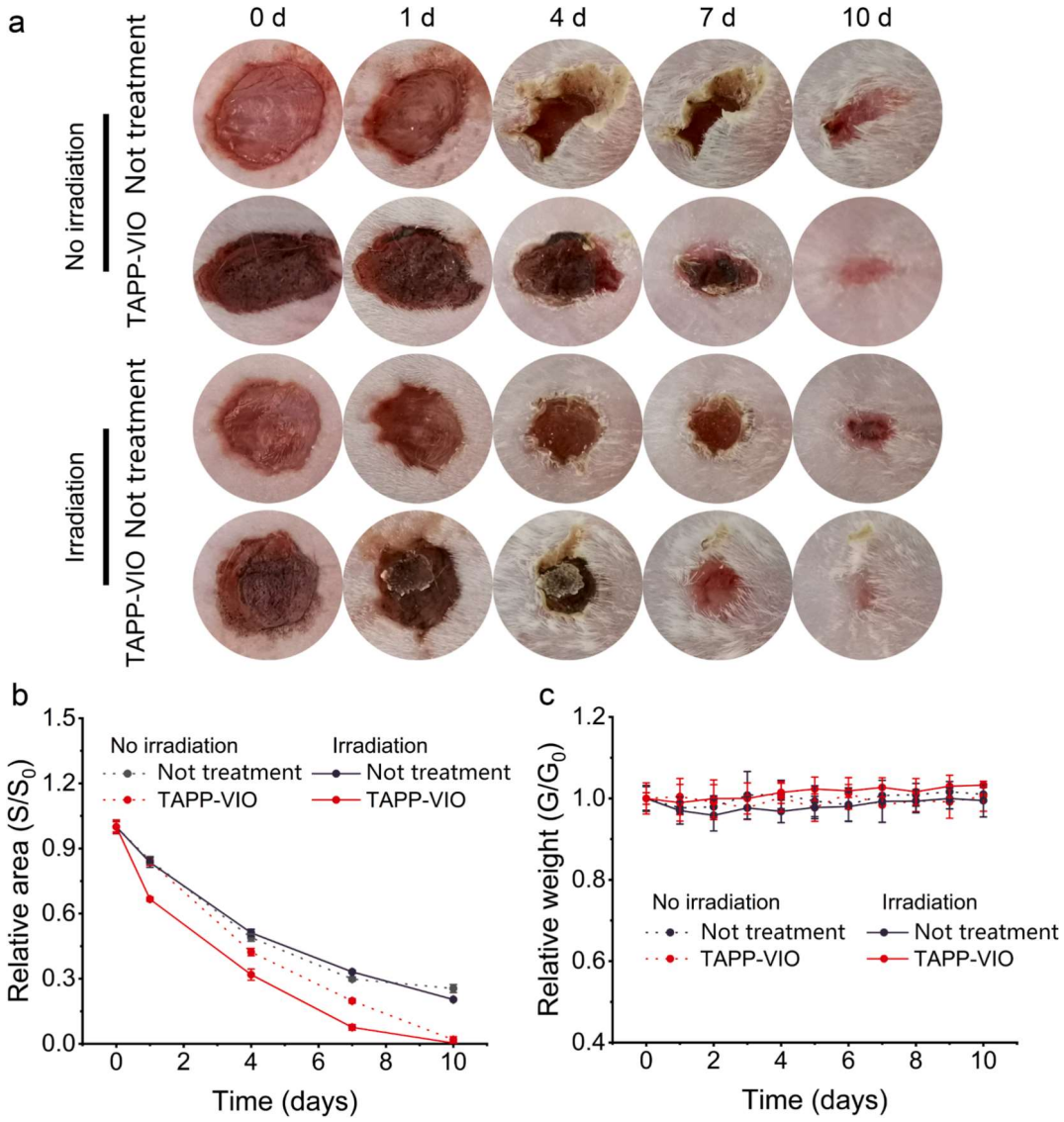

Fig. 4. (a) Enlarged photographs of local wounds in different groups of mice on days 0, 1, 4, 7 and 10. (b) The relative wound areas of the different groups at different time points. S and S_0 are the areas of the infected wound at a certain therapy point and before treatment, respectively. (c) Body weights of mice from different groups at different time points during the healing process. G_0 is the initial weight of mice, while G is the weight of treated mice at a certain therapy point.

As shown in Fig. 4a and Fig. S14, although the wounds in all treatment groups gradually decreased over time, the wound healing speed was faster and the healing degree was more pronounced in the TAPP-VIO treatment group, particularly in the group treated with TAPP-VIO combined with irradiation. On the 10th day after irradiation, the wounds of the TAPP-VIO + irradiation group had not only healed completely, but also presented a pink healthy skin. To provide a clearer comparison of healing progress, the relative area of the wound during the treatment process were recorded. As shown in Fig. 4b, during the whole observation process, the relative wound area of the TAPP-VIO and TAPP-VIO + irradiation groups were smaller than that of the control group, particularly TAPP-VIO with the irradiation group reaching a relative wound area of zero by the 10th day of treatment. These results indicate that TAPP-VIO can bind to bacteria alone and disrupt the bacterial membrane potential through electrostatic interaction. Meanwhile, TAPP-VIO generates heat and $^1O_2$ to synergically kill bacteria when illuminated, which plays a better role in promoting wound healing. Besides, monitoring the body weight, a key health indicator, revealed no significant fluctuations in any treatment group throughout the study, indicating that the TAPP-VIO has no significant side-effects (Fig. 4C).

To further evaluate the effects of different treatments on wound healing and inflammation in mice, H&E staining, Masson staining, and inflammatory factor (such as TNF-α and IL-6) staining were performed on the skin samples from the wound sites. As shown in Fig. 5, H&E and Masson staining revealed fewer inflammatory cells and more collagen tissue in the TAPP-VIO and TAPP-VIO + irradiation groups compared with the other treatment groups, suggesting superior wound healing in these two groups. Inflammatory factor staining (Fig. 5) also showed significantly reduced TNF and IL-6 levels in the TAPP-VIO treatment group, particularly in the TAPP-VIO combined with irradiation. These results indicate that TAPP-VIO can effectively bind to bacteria in the wound, inducing bacterial cell death. Moreover, the bactericidal effect of TAPP-VIO is further enhanced by irradiation, thereby promoting more efficient wound healing. In addition, no observable inflammatory reaction was observed in the H&E staining of the main organs of mice after treatment, indicating that TAPP-VIO combined with irradiation treatment has no obvious side effects on mice (Fig. S15).

4. Conclusions

In conclusion, the TAPP-VIO cationic COF integrates bacteria-targeting capabilities with phototherapy/chemotherapy synergistic bactericidal functions, demonstrating strong antibacterial effects and promoting wound healing ability. Through optimized hydrothermal synthesis, we obtained the porous nanomaterials with a well-defined crystal structure and large surface. The introduction of the ionic monomer VIO gives the material a certain interlayer electrostatic repulsion, effectively reducing the aggregation of porphyrin monomer caused by π-π stacking effect, and enhancing the production capacity of $^1O_2$. In addition, the relatively mild photothermal effect aids in bactericidal effect while minimizing thermal damage to adjacent tissues. The cationic VIO monomer also facilitates active bacterial-targeting and enhances the bactericidal effect through chemotherapy. Both *in vitro* and *in vivo* studies confirmed that TAPP-VIO exhibits strong bacterial binding affinity and a robust synergistic bactericidal effect, effectively promoting the healing of infected wounds. Furthermore, TAPP-VIO shows good cell compatibility and good application prospect. The design of this cationic framework material provides a new idea for the design of nano photosensitizers and bactericidal drugs.

CRediT authorship contribution statement

Jia-Jun Qian: Writing – original draft, Methodology, Investigation, Formal analysis, Data curation. **Jing-Xuan Guo:** Writing – review & editing, Validation, Supervision, Methodology, Investigation. **Meng-Chao Wang:** Validation, Formal analysis, Data curation. **Li-Jian Chen:** Validation, Formal analysis. **Xu Zhao:** Writing – review & editing, Supervision, Project administration, Investigation, Funding acquisition, Formal analysis, Conceptualization. **Xiu-Ping Yan:** Writing – review & editing, Supervision, Project administration, Funding acquisition.

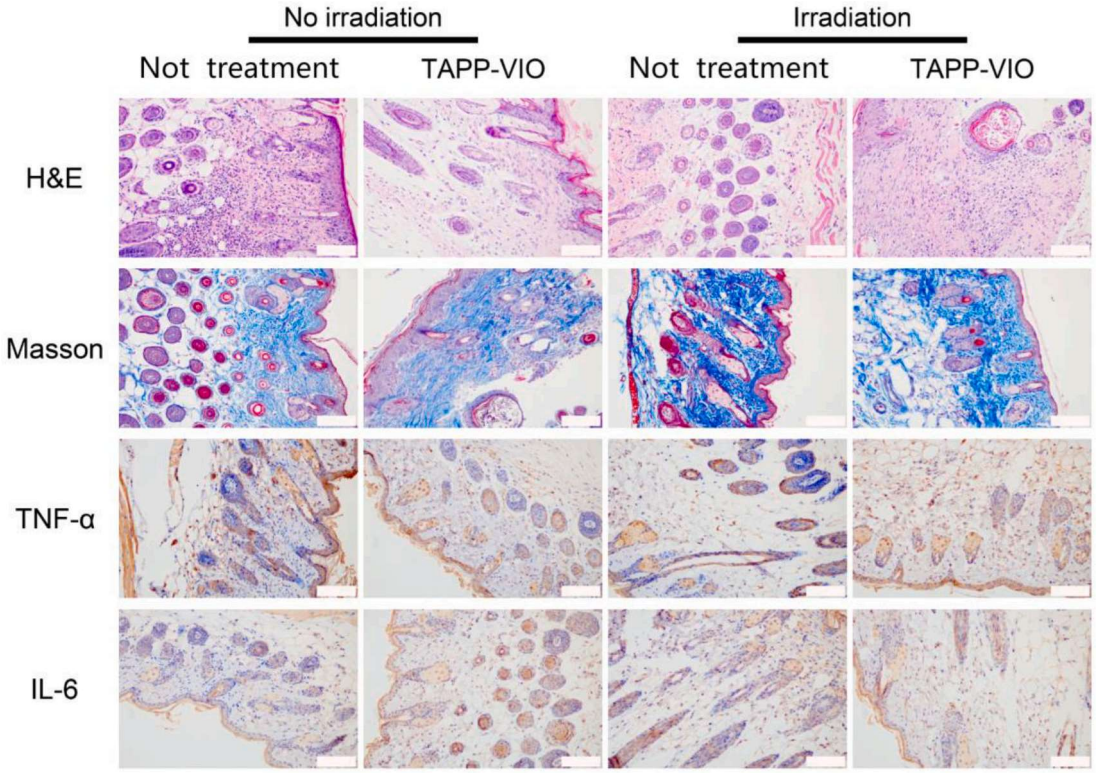

Fig. 5. The stained wound of mice after 10 days of different treatments (H&E, Masson, TNF-α and IL-6) (scale bar, 100 μm).

Declaration of competing interest

The authors declare that they have no known competing financial interests or personal relationships that could have appeared to influence the work reported in this paper.

Acknowledgements

This work was supported by Basic Research program of Jiangsu (No. BK20231491 and BK20180581) and the Collaborative Innovation Center of Food Safety and Quality Control in Jiangsu Province.

Appendix A. Supplementary data

Supplementary data to this article can be found online at https://doi.org/10.1016/j.jcis.2025.137494.

Data availability

No data was used for the research described in the article.

References

[1] H. Sorg, D.J. Tilkorn, S. Hager, J. Hauser, U. Mirastschijski, Skin wound healing: an update on the current knowledge and concepts, Eur. Surg. Res. 58 (1–2) (2017) 81–94, https://doi.org/10.1159/000454919.
[2] M. Cully, Nosing around for new antibiotics, Nat. Rev. Drug Discov. 15 (9) (2016) 604, https://doi.org/10.1038/nrd.2016.170.
[3] A. York, Bacterial evolution historical influences on antibiotic resistance, Nat. Rev. Microbiol. 15 (10) (2017) 576, https://doi.org/10.1038/nrmicro.2017.111.
[4] Y. Zhao, Q. Guo, X. Dai, X. Wei, Y. Yu, X. Chen, C. Li, Z. Cao, X. Zhang, A biomimetic non-antibiotic approach to eradicate drug-resistant Infections, Adv. Mater. 31 (7) (2019) 1806024, https://doi.org/10.1002/adma.201806024.
[5] I. Cavallo, F. Sivori, A. Mastrofrancesco, E. Abril, M. Pontone, E.G. Di Domenico, F. Pimpinelli, Bacterial biofilm in chronic wounds and possible therapeutic approaches, Biology 13 (2) (2024) 109, https://doi.org/10.3390/biology13020109.
[6] Y. Song, R. Wang, Y. Pan, D. Fang, Y. Tian, S. Zhou, An integrated quorum quenching biocatalytic nanoplatform for synergistic chemo-photothermal eradication of P. aeruginosa biofilm infections, Acta Biomater. 171 (2023) 532–542, https://doi.org/10.1016/j.actbio.2023.09.021.
[7] C. Yu, S. Sui, X. Yu, W. Huang, Y. Wu, X. Zeng, Q. Chen, J. Wang, Q. Peng, $Ti_3C_2T_x$ MXene loaded with indocyanine green for synergistic photothermal and photodynamic therapy for drug-resistant bacterium, Colloid Surf. B-Biointerfaces 217 (2022) 112663, https://doi.org/10.1016/j.colsurfb. 2022.112663.
[8] Y. Chen, Y. Gao, Y. Chen, L. Liu, A. Mo, Q. Peng, Nanomaterials-based photothermal therapy and its potentials in antibacterial treatment, J. Control. Release 328 (2020) 251–262, https://doi.org/10.1016/j.jconrel.2020.08.055.
[9] C. Li, F. Gao, Y. Tong, F. Chang, H. Han, C. Liu, M. Xu, H. Li, J. Zhou, X. Li, F. Wang, Y. Jiang, NIR-II window triple-mode antibacterial nanoplatform: cationic copper sulfide nanoparticles combined vancomycin for synergistic bacteria eradication, J. Colloid Interface Sci. 628 (2022) 595–604, https://doi.org/10.1016/j.jcis.2022.08.086.
[10] L. Guo, Y. Tian, L. Zhou, S. Kang, C. Zhang, W. Liu, H. Diao, L. Feng, Tailored phototherapy agent by infection site In situ activated against methicillin-resistant S. aureus, Adv. Healthc. Mater. 13 (2024) 2400593, https://doi.org/10.1002/adhm.202400593.
[11] Q. Xin, H. Shah, A. Nawaz, W. Xie, M.Z. Akram, A. Batool, L. Tian, S.U. Jan, R. Boddula, B. Guo, Q. Liu, J.R. Gong, Antibacterial carbon-based nanomaterials, Adv. Mater. 31 (45) (2019) 1804838, https://doi.org/10.1002/adma.201804838.
[12] B. Li, Y. Luo, Y. Zheng, X. Liu, L. Tan, S. Wu, Two-dimensional antibacterial materials, Prog. Mater Sci. 130 (2022) 100976, https://doi.org/10.1016/j.pmatsci.2022.100976.
[13] Y. Wang, Y. Yang, Y. Shi, H. Song, C. Yu, Antibiotic-free antibacterial strategies enabled by nanomaterials: progress and perspectives, Adv. Mater. 32 (18) (2020) 1904106, https://doi.org/10.1002/adma.201904106.
[14] J. Ghorbani, D. Rahban, S. Aghamiri, A. Teymouri, A. Bahador, Photosensitizers in antibacterial photodynamic therapy: an overview, Laser Ther. 27 (4) (2018) 293–302, https://doi.org/10.5978/islsm.27_18-RA-01.
[15] Y. Zheng, Y. Yan, L. Lin, Q. He, H. Hu, R. Luo, D. Xian, J. Wu, Y. Shi, F. Zeng, C. Wu, G. Quan, C. Lu, Titanium carbide MXene-based hybrid hydrogel for chemo-photothermal combinational treatment of localized bacterial infection, Acta Biomater. 142 (2022) 113–123, https://doi.org/10.1016/j.actbio. 2022.02.019.
[16] W. Li, J. Cai, W. Zhou, X. Zhao, M. Wang, X. Zhou, L. Ren, Poly(aspartic acid)-based self-healing hydrogel with precise antibacterial ability for rapid infected-wound repairing, Colloid Surf. B-Biointerfaces 221 (2023) 112982, https://doi.org/10.1016/j.colsurfb.2022.112982.
[17] A. Naskar, K.-S. Kim, Friends against the foe: synergistic photothermal and photodynamic therapy against bacterial infections, Pharmaceutics 15 (4) (2023) 1116, https://doi.org/10.3390/pharmaceutics15041116.
[18] V.-N. Nguyen, Z. Zhao, B.Z. Tang, J. Yoon, Organic photosensitizers for antimicrobial phototherapy, Chem. Soc. Rev. 51 (9) (2022) 3324–3340, https://doi.org/10.1039/D1CS00647A.
[19] J. Sun, L. Song, Y. Fan, L. Tian, S. Luan, S. Niu, L. Ren, W. Ming, J. Zhao, Synergistic photodynamic and photothermal antibacterial nanocomposite membrane triggered by single NIR light source, ACS Appl. Mater. Interfaces 11 (30) (2019) 26581–26589, https://doi.org/10.1021/acsami.9b07037.
[20] N. Li, G. Wu, L. Tang, W. Zhou, S. Yang, Q. Pan, M. Wang, P. Wu, H. Xiao, Y. He, X. Tan, Q. Yang, Metabolic labeling strategy boosted antibacterial efficiency for photothermal and photodynamic synergistic bacteria-infected wound therapy, ACS Appl. Mater. Interfaces 14 (41) (2022) 46362–46373, https://doi.org/10.1021/acsami.2c15759.
[21] X. Cai, J. Tian, J. Zhu, J. Chen, L. Li, C. Yang, J. Chen, D. Chen, Photodynamic and photothermal co-driven CO-enhanced multi-mode synergistic antibacterial nanoplatform to effectively fight against biofilm infections, Chem. Eng. J. 426 (2021) 131919, https://doi.org/10.1016/j.cej.2021.131919.
[22] K. Bilici, N. Atac, A. Muti, I. Baylam, O. Dogan, A. Sennaroglu, F. Can, H.Y. Acar, Broad spectrum antibacterial photodynamic and photothermal therapy achieved with indocyanine green loaded SPIONs under near infrared irradiation, Biomater. Sci. 8 (16) (2020) 4616–4625, https://doi.org/10.1039/d0bm00821d.
[23] X. Kang, X. Yang, F. Bu, W. Feng, F. Liu, W. Xie, G. Li, X. Wang, GSH/pH cascade-responsive nanoparticles eliminate methicillin-resistant staphylococcus aureus biofilm via synergistic photo-chemo therapy, ACS Appl. Mater. Interfaces 16 (3) (2024) 3202–3214, https://doi.org/10.1021/acsami.3c17198.
[24] B. Luo, Y. Xiong, J. Cai, R. Jiang, Y. Li, C. Xu, X. Wang, Chitin-assisted synthesis of CuS composite sponge for bacterial capture and near-infrared-promoted healing of infected diabetic wounds, ACS Appl. Mater. Interfaces 16 (38) (2024) 50160–50174, https://doi.org/10.1021/acsami.4c07586.
[25] Q. Xu, Q. Li, M. Ding, W. Xiu, B. Zhang, Y. Xue, Q. Wang, D. Yang, H. Dong, Z. Teng, Y. Mou, Flexible nanoplatform facilitates antibacterial phototherapy by simultaneously enhancing photosensitizer permeation and relieving hypoxia in bacterial biofilms, Acta Biomater. 184 (2024) 313–322, https://doi.org/10.1016/j.actbio.2024.06.018.
[26] B. Luan, X. Chu, Y. Wang, X. Qiao, Y. Jiang, F. Zhang, Construction of COF/COF organic s-scheme heterostructure for enhanced overall water splitting, Adv. Mater. 36 (2024) 2412653, https://doi.org/10.1002/adma.202412653.
[27] L. Song, W. Gao, S. Jiang, Y. Yang, W. Chu, X. Cao, B. Sun, L. Cui, C. Zhang, One-dimensional covalent organic framework with improved charge transfer for enhanced electrochemiluminescence, Nano Lett. 24 (21) (2024) 6312–6319, https://doi.org/10.1021/acs.nanolett.4c01074.
[28] W. Yang, Y. Du, B. Liu, Novel environmentally friendly covalent organic framework/polylactic acid composite material with high chemical stability for sand-control material, Polymers 15 (7) (2023) 1659, https://doi.org/10.3390/polym15071659.
[29] L. Xin, C. Zhang, J. Chen, Y. Jiang, Y. Liu, P. Jin, X. Wang, G. Wang, P. Huang, Ultrasound-activatable phase-shift nanoparticle as a targeting antibacterial agent for efficient eradication of pseudomonas aeruginosa biofilms, ACS Appl. Mater. Interfaces 14 (42) (2022) 47420–47431, https://doi.org/10.1021/acsami.2c13166.
[30] L. Cai, C. Hu, S. Liu, Y. Zhou, M. Pang, J. Lin, A covalent organic framework-based multifunctional therapeutic platform for enhanced photodynamic therapy via catalytic cascade reactions, Sci. China-Mater. 64 (2) (2021) 488–497, https://doi.org/10.1007/s40843-020-1428-0.
[31] L. Guoliang, W. Aying, L. Jianghua, W. Di, W. Yongning, Facile extraction and determination of organophosphorus pesticides in vegetables via magnetic functionalized covalent organic framework nanocomposites, Food Chem. 337 (2021) 127974, https://doi.org/10.1016/j.foodchem.2020.127974.
[32] Q. Guan, L. Zhou, L. Zhou, M. Li, G. Qin, W. Li, Y. Li, Y. Dong, A carbon nanomaterial derived from a nanoscale covalent organic framework for photothermal therapy in the NIR-II biowindow, Chem. Commun. 56 (56) (2020) 7793–7796, https://doi.org/10.1039/d0cc00861c.
[33] F. Liu, C. Nie, Q. Dong, Z. Ma, W. Liu, M. Tong, AgI modified covalent organic frameworks for effective bacterial disinfection and organic pollutant degradation under visible light irradiation, J. Hazard. Mater. 398 (2020) 122865, https://doi.org/10.1016/j.jhazmat.2020.122865.
[34] N. Mokhtari, M. Dinari, F. Khosravi Esmaeiltarkhani, Imine-linked covalent organic frameworks: a biocompatible and pH-dependent carrier for in vitro sustained release of doxorubicin, ACS Omega 8 (28) (2023) 25565–25573, https://doi.org/10.1021/acsomega.3c03316.
[35] S. Zhou, T. Tian, T. Meng, J. Wu, D. Hu, Q. Liao, J. Zhuang, H. Wang, G. Zhang, Tumor-derived covalent organic framework nanozymes for targeted chemo-photothermal combination therapy, iScience 26 (8) (2023) 107348, https://doi.org/10.1016/j.isci.2023.107348.
[36] J. Feng, S. Yang, Y. Shao, Y. Sun, Z. He, Y. Wang, Y. Zhai, Y. Dong, Covalent organic framework-based nanomotor for multimodal cancer photo-theranostics, Adv. Healthc. Mater. 12 (2023) 2301645, https://doi.org/10.1002/adhm.202301645.
[37] S. Zhang, S. Xia, L. Chen, Y. Chen, J. Zhou, Covalent organic framework nanobowls as activatable nanosensitizers for tumor-specific and ferroptosis-augmented sonodynamic therapy, Adv. Sci. 10 (6) (2023), https://doi.org/10.1002/advs.202206009 e2206009.

[38] L.A. Baldwin, J.W. Crowe, D.A. Pyles, P.L. McGrier, Metalation of a mesoporous three-dimensional covalent organic framework, J. Am. Chem. Soc. 138 (46) (2016) 15134–15137, https://doi.org/10.1021/jacs.6b10316.
[39] R. Liu, K.T. Tan, Y. Gong, Y. Chen, Z. Li, S. Xie, T. He, Z. Lu, H. Yang, D. Jiang, Covalent organic frameworks: an ideal platform for designing ordered materials and advanced applications, Chem. Soc. Rev. 50 (1) (2021) 120–242, https://doi.org/10.1039/d0cs00620c.
[40] J. Zeng, X. Wang, B. Xie, M. Li, X. Zhang, Covalent organic framework for improving near-infrared light induced fluorescence imaging through two-photon induction, Angew. Chem. Int. Ed. 59 (25) (2020) 10087–10094, https://doi.org/10.1002/anie.201912594.
[41] J. Zou, J. Zhu, Z. Yang, L. Li, W. Fan, L. He, W. Tang, L. Deng, J. Mu, Y. Ma, Y. Cheng, W. Huang, X. Dong, X. Chen, A phototheranostic strategy to continuously deliver singlet oxygen in the dark and hypoxic tumor microenvironment, Angew. Chem. Int. Ed. 59 (23) (2020) 8833–8838, https://doi.org/10.1002/anie.201914384.
[42] M. Zhang, J. Fang, Y. Liu, Y. Wang, L. Liao, L. Tang, L. Zhu, S. Qiu, Q. Fang, 3D covalent organic frameworks based on polycyclic aromatic hydrocarbons for reversible oxygen capture, Small Struct. 2 (4) (2021) 2000108, https://doi.org/10.1002/sstr.202000108.
[43] L. Zhang, S. Wan, J. Zhang, M. Zhang, Q. Yang, B. Zhang, W. Wang, J. Sun, R.T. K. Kwok, J.W.Y. Lam, H. Deng, Z. Sun, B.Z. Tang, Activation of pyroptosis using AIEgen-based sp2 carbon-linked covalent organic frameworks, J. Am. Chem. Soc. 145 (32) (2023) 17689–17699, https://doi.org/10.1021/jacs.3c04027.
[44] Q. Yue, J. Yu, Q. Zhu, D. Xu, M. Wang, J. Bai, N. Wang, W. Bian, B. Zhou, Polyrotaxanated covalent organic frameworks based on β-cyclodextrin towards high-efficiency synergistic inactivation of bacterial pathogens, Chem. Eng. J. 486 (2024) 150345, https://doi.org/10.1016/j.cej.2024.150345.
[45] J. Wu, T. Meng, X. Zhang, S. Tang, L. Liu, J. Xue, X. Liu, J. Wang, J. Wen, D. Hu, G. Zhang, Glucose-responsive Zn(II)-porphyrin COF adhesive hydrogels with dual-active sites and GOX-like activity for accelerated wound healing, Adv. Healthc. Mater. 14 (2025) 2404076, https://doi.org/10.1002/adhm.202404076.
[46] Y. Zou, Y. Qi, X. Li, H. Long, Z. Jia, N. He, J. Zhang, N. Liu, Y. Li, L. Ma, Simple and efficient hydrogen bond-assisted unit exchange for constructing highly soluble covalent organic frameworks, ACS Macro Lett. 12 (9) (2023) 1237–1243, https://doi.org/10.1021/acsmacrolett.3c00438.
[47] R. Zhu, W. Han, Y. Liu, J. Fu, J. Feng, J. Zhang, H. Pang, Z. Gu, Mechanical interlocking induced emission in two-dimensional covalent organic frameworks, Chem. Eng. J. 483 (2024) 149174, https://doi.org/10.1016/j.cej.2024.149174.
[48] Z. Chen, Q. Zhan, Y. Yan, Y. Cai, Z. Yang, Covalent organic framework based nanocomposite for low temperature photothermal therapy, ChemistrySelect 9 (28) (2024), https://doi.org/10.1002/slct.202401909 e202401909.
[49] J. Guo, S. Kong, Y. Lian, M. Zhao, Recent bio-applications of covalent organic framework-based nanomaterials, Chem. Commun. 60 (8) (2024) 918–934, https://doi.org/10.1039/d3cc04368a.
[50] J.G. Hurdle, A.J. O'Neill, I. Chopra, R.E. Lee, Targeting bacterial membrane function: an underexploited mechanism for treating persistent infections, Nat. Rev. Microbiol. 9 (1) (2011) 62–75, https://doi.org/10.1038/nrmicro2474.
[51] K. Kim, W.C.W. Chen, Y. Heo, Y. Wang, Polycations and their biomedical applications, Prog. Mater Sci. 60 (2016) 18–50, https://doi.org/10.1016/j.progpolymsci.2016.05.004.
[52] I.O. Savelyeva, K.A. Zhdanova, M.A. Gradova, O.V. Gradov, N.Y.A. Bragina, Cationic porphyrins as antimicrobial and antiviral agents in photodynamic therapy, Curr. Issues Mol. Biol. 45 (12) (2023) 9793–9822, https://doi.org/10.3390/cimb45120612.
[53] M. Wang, J. Guo, L. Chen, X. Zhao, Acrylate-functionalized porphyrin-covalent organic framework for bacterial-targeted and reaction-enhanced synergistic phototherapy/chemotherapy toward sterilization and wound healing, Biomater. Sci. 11 (5) (2023) 1776–1784, https://doi.org/10.1039/d2bm01723g.
[54] T. Wang, C. Xue, X. Zhao, Y. Liu, Y. Wang, L. Shi, Q. Shuai, Single NIR laser-activated synergistic low-temperature photothermal therapy and self-oxygenated photodynamic therapy nano-platforms for bacteria infection, Dyes Pigment. 225 (2024) 112066, https://doi.org/10.1016/j.dyepig. 2024.112066.
[55] G. Ma, Z. Liu, C. Zhu, H. Chen, R.T.K. Kwok, P. Zhang, B.Z. Tang, L. Cai, P. Gong, H_2O_2-Responsive NIR-II AIE nanobomb for carbon monoxide boosting low-temperature photothermal therapy, Angew. Chem. Int. Ed. 61 (36) (2022), https://doi.org/10.1002/anie.202207213 e202207213.
[56] Y. Chen, T. Feng, X. Zhu, Y. Tang, Y. Xiao, X. Zhang, S. Wang, D. Wang, W. Wen, J. Liang, H. Xiong, Ambient synthesis of porphyrin-based Fe-covalent organic frameworks for efficient infected skin wound healing, Biomacromolecules 25 (6) (2024) 3671–3684, https://doi.org/10.1021/acs.biomac. 4c00261.
[57] S. Wang, J. Zhang, L. Chu, H. Xiao, C. Miao, Z. Pan, Y. Qiao, Z. Wang, B. Zhou, Crown-ether threaded covalent organic polyrotaxane framework (COPF) towards synergistic crown/Zn^{2+}/photothermal/photodynamic antibacterial and infected wound healing therapy, Biomater. Adv. 159 (2024) 213814, https://doi.org/10.1016/j.bioadv.2024.213814.
[58] F. Meng, H. Qian, X. Yan, Conjugation-regulating synthesis of high photosensitizing activity porphyrin-based covalent organic frameworks for photodynamic inactivation of bacteria, Talanta 233 (2021) 122536, https://doi.org/10.1016/j.talanta.2021.122536.